Journal of Immunological Methods 474 (2019) 112643

Contents lists available at ScienceDirect

Journal of Immunological Methods

journal homepage: www.elsevier.com/locate/jim

Research paper

Sensitivity and binding kinetics of an ultra-sensitive chemiluminescent enzyme-linked immunosorbent assay at arrays of antibodies

Carmen I. Tobos[a,1], Seunghyeon Kim[b,1], David M. Rissin[a,1], Joseph M. Johnson[a], Scott Douglas[a], Susan Yan[a], Shuai Nie[a], Bradley Rice[a], Ki-Joo Sung[b], Hadley D. Sikes[b], David C. Duffy[a,*]

[a] Quanterix Corporation, 900 Middlesex Turnpike, Billerica, MA 01821, USA
[b] Department of Chemical Engineering, Massachusetts Institute of Technology, 77 Massachusetts Avenue, Cambridge, MA 02139, USA

ABSTRACT

We have characterized the sensitivity and kinetics of a multiplex immunoassay system based on detection of chemiluminescence (CL) at arrays of antibodies. This enzyme-linked immunosorbent assay (ELISA) was based on the spotting of different antibodies in a circular pattern at the bottom of a well of a microtiter plate. Sandwich immunocomplexes within each spot were labeled with horse radish peroxidase, and CL was generated locally to each spot in the array from turnover of luminol substrate. CL from the arrays across the plate was collected in single images; long exposure times were used to maximize sensitivity, and short exposure times were used to extend the dynamic range at higher signals. Image analysis was used to determine the intensity of light from each spot in the array, and intensity was converted to concentration of protein via comparison to a calibration curve. To determine the intrinsic sensitivity of the CL ELISA array, streptavidin horseradish peroxidase (SA-HRP) was captured on an array spotted with biotinylated detection antibodies. The limit of detection (LOD) of SA-HRP was 105 aM, or 3200 enzymes per 50 µL. A single-plex assay for prostate specific antigen (PSA) was developed that had an LOD of 79 aM when the microtiter plate was shaken orbitally, comparable to the most sensitive immunoassays reported to date. Normalization of CL signals in the PSA assay to signal per molecule of SA-HRP showed that the efficiency of the shaken assay was ~40%. When the plates were not shaken, the efficiency was ~4.5%, i.e., ~9-fold lower than when shaken. To better understand the theoretical basis of the sensitivity of these assays, we developed COMSOL numerical models of the binding kinetics at the array for plates that were shaken orbitally and those not shaken. Experimental data from the orbitally shaken PSA assay were best modeled by inertial mixing in a three-layer system that included a 8-µm-thick concentration boundary layer. Experimental data from the unshaken PSA assay were well modeled by diffusion-limited kinetics. A single-plex assay for IL-10 was developed with an LOD of 69 aM or 1.5 fg/mL, and used to measure this cytokine in plasma and serum of 10 healthy individuals. A 5-plex assay for IL-5, IL-6, IL-10, IL-22, and TNF-α was developed with LODs of 56 aM, 237 aM, 69 aM, 88 aM, and 373 aM, respectively. The assay was used to measure these 5 cytokines in the plasma and serum of the same individuals. The correlation in concentration of IL-10 measured in single-plex and multiplex assays was good (r^2 = 0.89; bias = 14.5%). The factors that result in the high sensitivity of CL ELISA arrays—mostly high signal to noise ratio of extended chemiluminescent imaging—are discussed. This multiplex CL ELISA could be used for sensitive profiling of multiple proteins for in vitro diagnostics and biomarker detection in the development of therapeutics.

1. Introduction

The sensitive measurement of proteins is important in a number of disciplines, including diagnosis of disease, clinical research, and the development of therapeutics.(Cohen and Walt, 2019; Wild, 2013) Highly sensitive immunoassays allow disease to be detected as early as possible, and allow biomarkers to be measured in samples that are readily accessible, such as plasma and serum, where they may be present in lower concentrations compared to tissues. The ability to measure multiple proteins simultaneously (multiplex immunoassays) also provides significant benefits, and has been the focus of extensive research efforts.(Cohen and Walt, 2019; Rivnak et al., 2015) In particular, multiplexing increases the biological information available to researchers, while conserving volume of critical clinical samples and minimizing cost. Additionally, multiplexed panels of proteins allow more specific and biologically-relevant diagnostic tests to be developed based on multi-variant analyses.(McDonald and Parsons, 2016) Immunoassay systems that measure multiple proteins simultaneously with high sensitivity are, therefore, highly desirable. In this paper, we characterize the sensitivity of a multiplex immunoassay system based on arrays of spotted capture antibodies for performing the enzyme-linked immunosorbent assay (ELISA) using chemiluminescent detection.

The use of arrays of spotted capture antibodies for multiplex immunoassays was first described by Ekins et al. 30 years ago.(Ekins et al., 1989; Ekins and Chu, 1991) Since then, many groups have developed

* Corresponding author.
E-mail address: dduffy@quanterix.com (D.C. Duffy).
[1] These authors contributed equally to this work.

https://doi.org/10.1016/j.jim.2019.112643
Received 22 June 2019; Accepted 7 August 2019
Available online 08 August 2019

assays based on this approach, and several systems have been commercialized. For example, Schweitzer et al. described the readout of arrays of immunocomplexes by rolling circle amplification of detection antibodies labeled with oligonucleotides.(Schweitzer et al., 2000) Meso Scale Discovery Inc. (MSD) has pioneered the imaging of arrays of immunocomplexes labeled with electrochemiluminescence (ECL) tags, and have created a menu of highly validated multiplex assays. (Malekzadeh et al., 2017) Roche developed a multiplexed biomarker system called Immunological MultiParameter Chip Technology (IMPACT) based on arrays of capture antibodies on polystyrene chips and readout of detection antibodies labeled with fluorescent latex particles. (Claudon et al., 2008) This method enabled the researchers to detect down to 10 individual binding events in a single spot, resulting in limits of detection in the femtomolar range.(Chandra et al., 2011) Several groups have also developed assays based on readout of arrays of spotted antibodies using enzyme labels, i.e., multiplex planar ELISA.(Wiese et al., 2001) For example, Mendoza et al. reported a multiplex indirect ELISA based on spotting of antigens into a 96-well plate and readout using alkaline phosphatase.(Mendoza et al., 1999) Huang et al. have developed various antibody arrays formats that enable the measurement of large numbers of proteins, including several systems based on ELISA readout.(Wilson et al., 2015) This approach to multiplex immunoassays is attractive for several reasons. First, arrays can be manufactured straightforwardly using a number of different methods for depositing antibodies on surfaces. Second, the sensitive detection of labels is enabled by sensitive and high resolution optical and camera systems. Third, these assays can leverage the extensive capabilities for automating the processing of 96-well plates, enabling high throughput and precise assay systems.

Here, we characterize a multiplex ELISA system based on imaging of chemiluminescence (CL) at arrays of capture antibodies that was first reported in 2001.(Moody et al., 2001) Fig. 1 shows a schematic of the multiplex CL ELISA format. This approach was first described by Moody et al. at Pierce Endogen,(Moody et al., 2001) who reported a 7-plex of inflammatory cytokines with limits of detection (LOD) ranging from 0.4 to 1.6 pg/mL. In 2009, the technology was acquired by Aushon Biosystems who further improved the signal-to-background ratios of the assays by spotting the arrays using a solid pin printing technology. (Austin and Holway, 2011) Since the first report of this technology, the multiplex CL ELISA has been used to measure biomarkers in a range of therapeutic areas, resulting in > 100 publications.(Backen et al., 2009; O et al., 2017; Purushothama et al., 2018; Tarhini et al., 2014)

In the work described here, we set out to characterize the fundamental physicochemical properties of the multiplex CL ELISA in order to understand the basis of its sensitivity. As for other ELISA formats, the sensitivity of this assay is determined by three main factors. First, the efficiency of capturing the target molecules and labeling them with enzymes to form immunocomplexes ("*How many molecules are available to be detected?*"). Second, the ability to detect the enzyme labels that is determined by the signal-to-noise of the enzyme-generated product ("*How many molecules are needed to reach the detection limit?*"). Third, the ability to detect enzyme labels arising from specific interactions with target molecules over those that bind due to non-specific interactions ("*Is the assay specific to bound target molecules?*"). We have shown previously—neglecting specific backgrounds arising from interferences, such as heterophilic antibodies—that backgrounds in ELISA can be minimized by maximizing the sensitivity to enzyme allowing lower concentrations of labeling molecules to be used.(Rissin et al., 2010) As a consequence, in the work presented here, we focused on understanding the first two factors.

As the kinetics of protein capture in planar ELISA are diffusion limited, they are often viewed as intrinsically less sensitivity than bead-based ELISA, for example, that is not diffusion limited.(Rissin et al., 2010) Highly sensitive assays in CL ELISA can be achieved, however, and we were interested in theoretical models that could help our understanding of the physical basis of this sensitivity. In particular, we

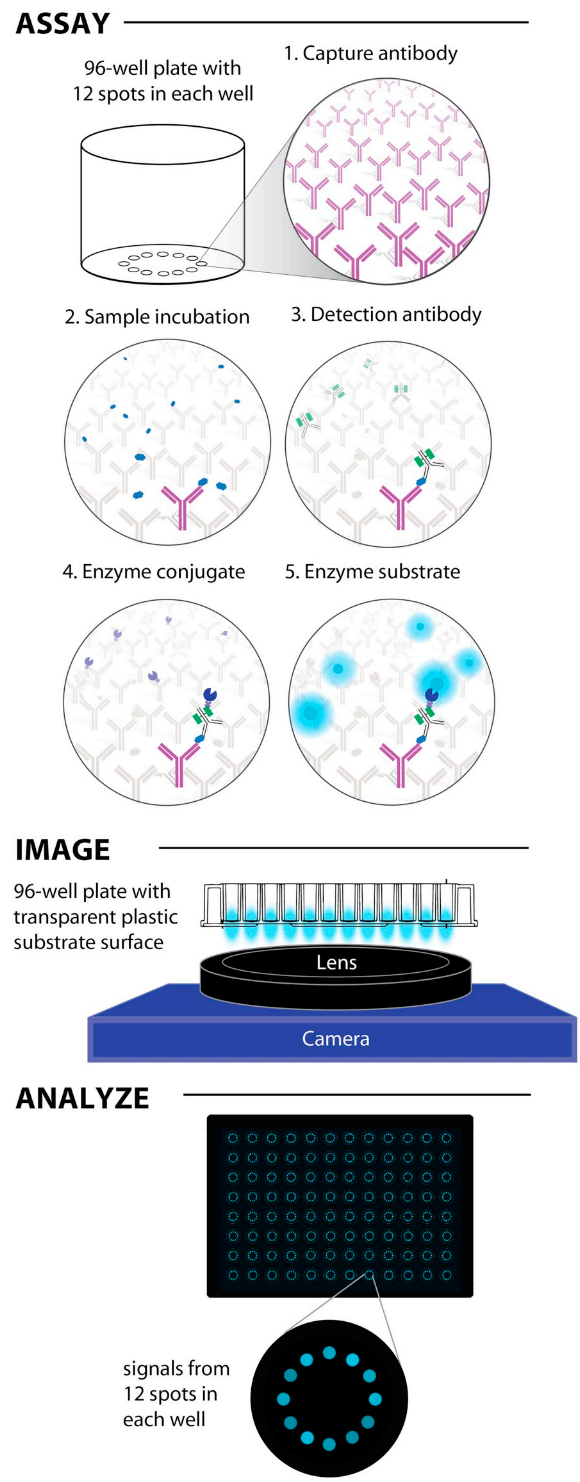

Fig. 1. Schematic diagram of the multiplex CL ELISA based on arrays of antibodies in microtiter plates.

wanted to predict how many molecules bind to the bottom of the well when the plate was shaken or static, as the kinetic limitations of planar ELISA are often overcome by actively mixing microtiter plates on orbital shakers. Orbital shaking results in complex flow, and kinetic models need to take into account both the fluid dynamics of mixing and binding kinetics driven by inter-molecular interactions. There are surprisingly few publications that quantitatively describe the mass transport and binding kinetics during the ELISA process in orbitally shaken microtiter plates. (Alpresa et al., 2018a; Alpresa et al., 2018b) We, therefore, developed kinetic models by using boundary layer theory (Schlichting et al., 2017) to simplify the effects of inertial mass transfer during the planar ELISA. The model development for the ELISA kinetics that we report should be instructive in general for ELISA as well as the specific format that was used here to test these models.

In this paper, we describe experimental and theoretical evaluations of: a) the factors that contribute to the signal-to-noise of the multiplex CL ELISA that determines the sensitivity to the enzyme label; and, b) the binding kinetics of the system that determine the number of enzyme labels that are available for detection. A deeper understanding of these two areas allowed us to optimize the sensitivity of the multiplex CL ELISA. We illustrated the improvement in sensitivity that was achieved using single-plex assays for PSA and IL-10, and a 5-plex assay for IL-5, IL-6, IL-10, IL-22, and TNF-α.

2. Materials and methods

2.1. Reagents

Arrays were created by depositing solutions of different antibodies (200–600 μg/mL) onto the bottom of polystyrene 96-well microtiter well plates (Thermo Fischer). The solutions were spotted using a contact printing process with solid stainless steel pins(Austin and Holway, 2011; Spurrier et al., 2008) of diameter 400 μm. The antibody spots were positioned in a circular pattern around the center of the well, and the resulting spot diameter was ~600 μm. After printing, the plates were dried, and a protein-based solution that reduced non-specific binding was added to each well. The plates were then thoroughly dried and sealed with desiccant packs. Sealed plates were stable for up to 5 years.

Calibrator solutions were made from commercially purchased antigens. Antigens were first reconstituted in a stabilization buffer. The concentration of the initially reconstituted antigen stock was compared to a known standard, and the reconstitution volume was adjusted to ensure a correct final concentration of the stock antigen. The stock antigen solution was diluted by the required dilution factor to create the calibrator with the highest concentration, and a series of calibrators were created via serial dilution.

Detection antibodies were exchanged into phosphate buffered saline (PBS) buffer, and biotinylated using an amine-reactive *N*-hydroxysuccinimidobiotin per standard protocols. The biotinylated antibodies were purified from excess biotin-reagent by dialysis into PBS. For multiplex assays, solutions of biotinylated detection antibodies were combined into mixtures. Solutions of detection antibodies were stored at either 4 °C or − 20 °C depending on the assay.

The enzyme conjugate, streptavidin horseradish peroxidase (SA-HRP) (Jackson ImmunoResearch Laboratories) was stored at −80 °C. HPLC analysis indicated that the molecular weight of the enzyme conjugate was ~113 kDa. Luminol—the substrate of the enzyme (Thermo Scientific)—was used according to manufacturer's instructions. Other components for assays (buffers, detergents, and blocking proteins) were used as received.

2.2. Assay steps

Antibody arrays on dried microtiter plates were reconstituted via washing with the Simoa plate washer (Quanterix Corporation). One wash consisted of 10 wash cycles, where each wash cycle dispensed and aspirated 300 μL of buffer per well, resulting in a 1.84×10^6-fold dilution factor. After the 10th wash cycle, no aspiration was performed. The residual wash buffer in the wells was removed by manual flicking the plate and firmly patting its top surface onto lint-free lab wipes. This wash protocol was used for all assay wash steps, with the exception of a final wash performed just prior to plate imaging. The final wash consisted of 4 washes, with three wash cycles each. After each of the four washes, the plate was manually flicked and patted dry to ensure all residual volume was removed from the wells.

Samples were diluted 4-fold in the appropriate sample diluent. 50 μL of calibrators or diluted samples were pipetted into wells of the washed plate. Plates were covered with lids to minimize evaporation, and were orbitally shaken at 525 rpm on the Simoa plate shaker (Quanterix Corporation) at 23 °C for 120 min. After sample incubation, plates were washed on the Simoa washer. 50 μL of biotinylated detection antibody was added to each well, and the plate was shaken at 525 rpm for 30 min at 23 °C. The plates were washed again, 50 μL of SA-HRP enzyme was added to each well, and the plate was shaken at 525 rpm for 30 min at 23 °C. The plate was washed again, and an additional final wash was executed. Luminol and hydrogen peroxide were mixed in a 1:1 ratio, and 50 μL of this solution was added to each well. The plates were imaged within 4 min of substrate addition.

For the SA-HRP assay (Section 3.4), a biotinylated PSA antibody (400 μg/mL) was deposited in the wells, blocked, and used to capture SA-HRP in a 1-step assay. 50 μL of various concentrations of SA-HRP was added to each well, and the plate was shaken at 525 rpm at 23 °C. Incubation of the enzyme conjugate was immediately followed by a standard wash cycle, substrate addition, and imaging.

For the unshaken PSA assay (Section 3.5.1), all three incubation steps were performed with plates at rest on a stationary benchtop. All other assay steps were the same as described above.

2.3. Imaging system and data analysis

After performing the assay steps, microtiter plates were read on the SP-X imager (Quanterix Corporation). Images were taken with both short and long exposure times to quantify high and low concentrations, respectively. Exposure times were optimized on an assay-specific basis to maximize sensitivity as determined by signal to background ratios. Short and long exposure times were 39 s and 741 s for the PSA and SA-HRP assay, and 46 s and 920 s for the IL-10 and 5-plex assays. Images were transferred to a personal computer, and analyzed using analysis software (Quanterix Corporation). The CL signal of each spot in an array was reported as the sum of intensity counts for each pixel within a circular region of interest (ROI). Long exposure images were used for quantitation as default, unless pixels saturated, in which case short exposure images were used. Data from the short exposure images were corrected to be equivalent to the long exposure time. The sum of signal from the ROI was finally divided by the long exposure time to yield a CL signal per second. CL signals as a function of concentrations of calibrators were fitted to a five parameter logistic fit (5PL). Sample concentrations were determined by extrapolating their CL signals from these calibration curves. The limits of detection (LOD) of an assay was calculated as the concentration corresponding to signal three standard deviations above assay background, assuming a 10% coefficient of variation (CV) at assay background. The lower limit of quantification (LLOQ) and upper limit of quantification (ULOQ) were determined as the lower and upper limits of the curve, respectively, where sample imprecision exceeded 20%, assuming a 10% coefficient of variation for assay signal. Dynamic range was determined from the difference in LLOQ and ULOQ.

2.4. Theoretical models

Reaction-diffusion equations and boundary conditions for planar ELISA were modeled using COMSOL Multiphysics® software, and numerically solved using backward differentiation formula (BDF) and parallel direct sparse solver (PARDISO). Simulations of the ELISA for PSA were run with a maximum time step of 1 s, and simulations for time course SA-HRP binding to a spotted biotinylated antibody were run with a maximum time step of 5 s.

3. Results and discussion

3.1. The multiplex chemiluminescent ELISA process

Fig. 1 shows a schematic of the multiplex CL ELISA used here. Different capture antibodies were deposited in distinct spots of the array to enable spatial encoding of specific immunocomplexes, thereby enabling multiplex detection. The arrays of capture antibodies were deposited in circular patterns, so that the transport to the individual capture spots were not affected by radial variation in flux of molecules to the surface.(United States Patent Application 13/677113, 2013) The surface of the array of capture antibodies was blocked with a solution of proteins that minimized non-specific binding and stabilized the arrays for storage. To perform an assay, a sample or calibrator was added to each well, and the microtiter plate was shaken at a controlled temperature, during which time the different target proteins were captured at the specific spot containing corresponding capture antibodies. The wells were washed and incubated with a mixture of detection antibodies labeled with biotin that formed sandwich immunocomplexes with the corresponding capture antibody-antigen complexes. The wells were washed again, and incubated with SA-HRP to label the immunocomplexes with enzymes. After a final wash, a chemilumigenic substrate (luminol) and H_2O_2 were added to each well so that the enzyme-substrate reaction yielded light emitted locally from the immunocomplexes. CL from the arrays was imaged on a CCD camera, and image analysis was used to determine the intensity of light emitted from each spot of the array in each well of the plate. Concentrations of proteins in samples were determined by comparison of intensity of spots from known concentrations of proteins in calibrator solutions. The concentrations of samples was determined by extrapolation of the signal from a fitted curve to the calibration concentration vs. CL signal data.

An innovation introduced by Honkanen et al.[25] was to array the antibodies in circular patterns centered on the middle of each well to improve the spot-to-spot precision of the CL signals. Orbital shaking results in a circular vortex within the well, and these authors hypothesized that the vortex results in a radial variation in flux of molecules to the surface resulting in the observed decrease in signal for spots arrayed close to the center of the well.(United States Patent Application 13/677113, 2013) The spot-to-spot signal variation in conventional arrays—which are spotted on a rectangular grid—is high, as each spot is a different distance from the center of the well. The array spots in the assay characterized here were the same radial distance from the center of the well, and away from the depletion region observed in the center of the well. As a result, the circular arrays resulted in better precision in spot-to-spot signals and higher signals in general, both resulting in improved sensitivity of the assay.

3.2. Generating and imaging CL at arrays

The imaging of CL generated from the enzyme-labeled immunocomplexes is a major factor in the high sensitivity of the assay characterized here. CL is a very high signal-to-noise optical effect used in many diagnostic systems to maximize sensitivity.(Weeks et al., 2013) This detection method does not require excitation light—and consequently no filters to remove this light—so in theory there is no background light for the specific CL emitted light to exceed, resulting in a very high signal-to-noise ratio (SNR). Furthermore, the use of enzyme labels creates thousands of chemiluminescent molecules per second, further increasing SNR over methods that use detection antibodies conjugated to a small number of chemiluminescent labels. The sensitivity of CL ELISA is, therefore, determined by efficiency of the detection system for capturing and detecting the emitted photons from the chemiluminescent products produced by the enzyme-substrate reaction, and by the effectiveness of minimizing photons that do not arise from the chemiluminescent product molecules.

The enzymatic reaction between HRP, its substrates, and H_2O_2 has been extensively studied for the last 50 years,(Veitch, 2004) including kinetic analysis of single enzymes.(Gorris and Walt, 2009) The reaction of HRP with luminol—the chemilumigenic substrate used here—is well understood.(Cormier and Prichard, 1968) The catalytic reaction is complex involving several intermediates, and is commonly modeled using 4 or more kinetic constants. Based on these kinetic models and the conditions used in the assay presented here, a steady state concentration of chemiluminescent product is rapidly produced by enzymes at the surface of the array that will drop as the substrate is consumed. Cormier et al.(Cormier and Prichard, 1968) showed that luminol-derived CL radicals last about 10 s in a mixture consisting of luminol, HRP, and H_2O_2. As the mean distance diffused by a molecule in time t is $\sqrt{4Dt/\pi}$, where D is the diffusion constant ($= 6.6 \times 10^{-6}\ cm^2/s$ for luminol),(Vitt et al., 1991) the average distance diffused in a lifetime is about 92 µm, equivalent to < 2 pixels in an image (see below). We would expect, therefore, that the CL signal is confined to within a pixel or two of the edge of the spot.

CL from the arrays of immunocomplexes on the microtiter plate was imaged onto a CCD camera. Light emitted through the transparent bottoms of all of the wells of the microtiter plate was collected by a lens (numerical aperture = 0.02), and imaged onto a cooled 3.2 Mp CCD camera. The resulting image had a resolution of ~46 µm per pixel. The approach of imaging the entire set of wells simultaneously leads to faster read times and higher throughput compared to methods that image wells one at a time. The rapid read time from imaging the entire plate has the additional benefit of allowing very long exposure times to maximize SNR from the enzyme and, consequently, assay sensitivity (see section 3.4), without requiring very long read times for the entire plate. Imaging emitted light through the optically flat bottom of the microtiter plate also likely improves SNR over approaches that image light through the meniscus of the liquid overlying the well surface that can lead to scattering of light, lower collection efficiency, and greater noise.

To maximize the sensitivity and dynamic range of the assay, we used two images at different exposure times, as described previously. (US Patent 8, 811, 704, 2014) Shorter exposure times (< 1 min) allowed higher concentrations of enzyme labels at the surface to be imaged without causing the camera to saturate. Longer exposure times (> 5 min) allowed integration of CL signals arising from low concentrations of bound enzymes in order to distinguish enzyme-specific signals over camera noise to maximize sensitivity. There were diminishing returns in imaging > 15 min due to the gradual increase in camera noise associated with dark current and the gradual decrease in CL signal as substrate is consumed. The data presented in Section 3.4 represent optimal exposure times to maximize sensitivity and dynamic range to enzyme for the imager used here.

3.3. Image analysis and quantitation

Images were analyzed to determine the CL signal from each spot of the array. First, camera dark current was removed by normalization of the images to stored calibration images obtained previously with the camera shutter closed. Dark current corrected images were then corrected for flat field effects using a mathematical model of lens distortion. The location of the CL spots arising from each element of the array was determined by first placing an initial grid of circular regions of interest (ROI; 12 per well; diameter = 12 pixels). The ROI was chosen to be smaller (diam. ≈ 550 µm) than the spot size (diam. ≈ 600 µm) to maximize signals without introducing false background signals. The position of each ROI was then optimized to maximize signal, with restrictions placed on the movement of the ROI to avoid false positive signals. The CL signal was determined as the sum of signal from the pixels in the ROI, with pixels whose center were less than the 6 pixel radius, resulting in 104 pixels per ROI. The summed CL signal was divided by the long exposure time to yield CL counts per second for each spot.

3.4. Limit of detection and dynamic range of enzyme labels at CL ELISA arrays

To establish a measurement of the intrinsic sensitivity of the CL ELISA arrays—and answer the question "*how many molecules are needed to reach our detection limit?*"—we developed an assay to determine the number of enzymes required to reach the detection limit of the imager. We have previously used a similar approach to determine the sensitivity to an enzyme label of the digital ELISA method that is based on single molecule arrays (Simoa).(Rissin et al., 2010) In that assay, we used biotinylated beads to capture and detect individual molecules of streptavidin-β-galactosidase (SβG). The limit of detection (LOD) of the bead based Simoa assay was [SβG] = 220 zM for a 4 h incubation time, equivalent to about 13 enzymes in a 100 μL sample. Here, we deposited 17 nL of 0.4 g/L biotinylated anti-PSA antibody (~3 biotins per antibody molecule) in a single spot on the surface of each of the wells of a 96-well plate. We then incubated each well with a known concentration of SA-HRP enzyme label, and detected the bound enzymes by CL. Fig. S1 shows a time course of the binding of 35 fM SA-HRP to the biotinylated antibody: the solutions containing enzyme needed to be incubated for approximately 1 day to reach equilibrium. Fits to these time course data indicated that the capture efficiency of SA-HRP was ~59.4% after the 5 h incubations that were subsequently tested.

The primary variable for increasing sensitivity of the CL assay was to increase exposure time in order to maximize the collection of photons, and increase the signal-to-background ratio. Fig. 2 shows the signal-to-background ratio and CL counts per second per molecule at different exposure times and a 5 h incubation of 17.7 fM SA-HRP. Signal-to-background increased with exposure time, and was maximized at exposure times > 500 s. CL counts per second per molecule was fairly constant with exposure time, with a maximum at 500 s. Fig. S2 shows CL signal for 10 consecutive 100 s exposures at several concentrations of SA-HRP. CL signals decrease with time, although the slope is consistent over the concentration range of SA-HRP, with reductions in signal per second of 25–36% for the 10th image compared to the 1st.

Based on these data, we selected an exposure time (741 s) to ensure a robust signal-to-background ratio, and generated a calibration curve of SA-HRP for a 5 h incubation time. Fig. 3 shows a plot of CL signal against [SA-HRP] bound to the arrayed biotinylated antibody for [SA-HRP] from 49 aM to 17.7 nM. The LOD of this experiment was 99 aM, and the average LOD from 5 runs was 105 aM, or about 3200 enzymes in 50 μL. This sensitivity is similar to those previously reported for CL immunoassays,(Rissin et al., 2010; Chen et al., 2017) and is about 500-fold less sensitive to enzyme than the Simoa assay using a similar incubation time.(Rissin et al., 2010) Based on a 59.4% capture efficiency after a 5 h incubation (Fig. S1), the number of enzymes captured from 50 μL and detected at the array was about 1900. Sensitivity to ~100 aM enzyme labels is sufficient to detect sub-femtomolar levels of proteins in solution, assuming high capture and labeling efficiencies (see Section 3.5).

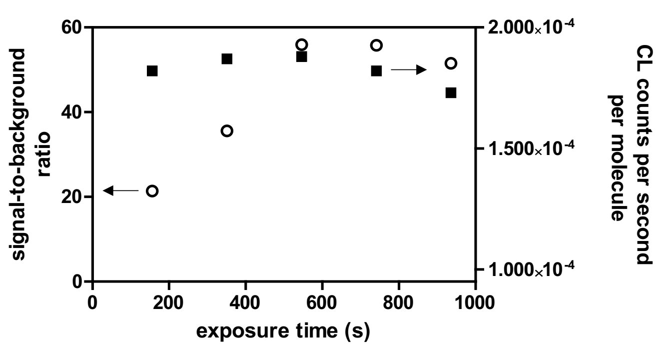

Fig. 2. Plots of signal-to-background ratio (open circles) and CL counts per second per molecule (solid squares) against exposure time for 17.7 fM SA-HRP incubated with a spotted biotinylated antibody.

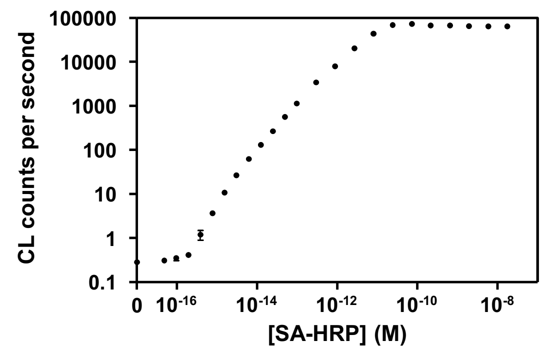

Fig. 3. Plot of CL counts per second against concentration of SA-HRP incubated with a spotted biotinylated antibody. As with other figures in this paper, error bars are shown and represent one standard deviation over triplicate measurements. In cases where error bars are not visible, they are smaller than the symbol. As with other figures in this paper with a log scale for concentration, the zero concentration or background signal is plotted on the intercept with the y-axes.

Fig. 3 also illustrates the dynamic range of the CL ELISA. At concentrations of SA-HRP greater than about 22 pM, the camera saturated during the short exposure (39 s), limiting the high end dynamic range. The LLOQ was 120 aM and the ULOQ was 9 pM, a dynamic range of 4.9 logs. The dynamic range could be extended by adding additional, shorter exposure times.

To enable us to quantify the number of molecules detected from the CL signals in immunoassays (Section 3.5.1), we needed to determine the CL signal per second generated by each molecule of SA-HRP. Fig. S3 shows a plot of CL signal per second per molecule at the different concentrations of SA-HRP measured in the model binding assay shown in Fig. 3, assuming capture of 59.4% of the enzymes in solution (Fig. S1), as predicted when the concentration of the biotinylated capture antibody is much greater than the concentration of SA-HRP. Three distinct regions are observed in this plot. At [SA-HRP] > 0.3 pM, the signal from the CCD was saturated, so the calculated signal per molecule drops with increasing [SA-HRP]. At [SA-HRP] < 0.4 fM, signals are close to background and do not vary significantly. At these high and low concentrations, signal per molecule and, therefore, the number of molecules detected cannot be determined reliably. Between these two extremes, signal per molecule increased with [SA-HRP] (Fig. S3B), reaching a maximum of 6.48×10^{-4} counts per molecule per second at 0.3 pM. This variation in signal per molecule is consistent with the mechanism of CL where two luminol radicals—generated in separate steps of the HRP-luminol-H_2O_2 reaction at different rates—are required for emission of a photon, so the kinetics are non-linear.(Cormier and Prichard, 1968) Due to this variation, we fitted the plot of CL signal per second per molecule against CL signal per second (Fig. S3B), and extrapolated values for CL signal per second per molecule for a given CL signal.

The sensitivity to enzyme in the CL ELISA array was limited by the signal-to-noise of the detection system. From the images used to generate the data in Fig. 3**,** there was no difference in CL intensity of wells containing substrate but no enzyme, and wells containing no substrate or enzyme, i.e., there was no measureable CL background signal. Sensitivity was, therefore, limited by the light collection optics and the noise of the CCD camera. For long images, the intrinsic noise (read noise and dark current noise) of the camera was ~6.5 counts. The noise associated with an ROI measurement consisting of 104 pixels is given by the square root of the pixel count times the camera noise, or 66 counts. If we define the limit of detection as S/N ~ 5 (CV ~ 20%), then we require an ROI signal of ~330 counts. Close to the detection limit, each enzyme produces approximately 0.179 counts over the course of a 741 s exposure (assuming 2.42×10^{-4} counts per molecule per second for a 5 h incubation (Fig. S3B)). We would expect, therefore, that ~1840 enzymes were required to exceed the background of the optical system, close to the number of enzymes detected at the surface at the LOD (1900). The signal-to-noise of the detection system and, consequently, the sensitivity of the assay could be improved by increasing the efficiency of light collection of the optics and using a camera with lower noise.

3.5. Kinetics of capture and labeling of target molecules in CL ELISA arrays

To understand the efficiency of capture of target molecules and their subsequent labeling with enzymes, i.e., to answer the question "*how many molecules are available to be detected?*", we developed experimental and theoretical models to determine the number of enzyme labels available for detection at the array surface. These theoretical models help to explain the physical basis of the high sensitivity of the ELISA that is diffusion-limited. The experimental data and theoretical models are described in turn, followed by a comparison of the two.

3.5.1. Experimental data

The number of enzyme labels specifically associated with immunocomplexes at the surface of the array is determined by the intermolecular binding kinetics during the various steps of the assay. We previously developed a kinetic model of another sensitive immunoassay—the Simoa digital ELISA assay—and demonstrated good concordance between the predicted number of molecules detected and experimental data.(Chang et al., 2012) For that particular assay, the capture antibodies were attached to microscopic beads and evenly distributed throughout the sample, such that each protein was within a distance of ~58 μm of the capture surface, and diffusion was sufficient for target molecules to reach the capture surface in short times (< 1 min). As a result, the kinetics were equivalent to a well-mixed system, and could be modeled using a simple biomolecular equation. In the case of an ELISA at the surface of the bottom of a well, however, the capture antibodies are not well distributed throughout the sample, and proteins are, on average, a significant distance from the capture surface: diffusion of those molecules to the bottom of the well becomes kinetically limiting. For example, protein molecules at the top of a 50 μL sample in the well are a distance of 1.6 mm from the capture antibodies at the bottom of a well. The time for a molecule to diffuse a mean distance $< x >$ is given by $\pi < x >^2/4D$, where D is the diffusion coefficient of the protein. For prostate specific antigen (PSA), $D = 8.5 \times 10^{-7}$ cm^2/s,(Chang et al., 2012) so a PSA molecule at the top of the sample will, therefore, take approximately 6.6 h to reach the capture surface by diffusion. This time is in contrast to the bead assay where each PSA molecule was within 31 s of diffusion to capture antibodies.(Chang et al., 2012) As a result, the CL array assay is limited by diffusion, and active methods for transporting the target molecules to the capture antibodies are required to achieve high capture efficiencies and sensitive assays.

The solution to the diffusion problem for the CL ELISA array is to shake the wells so that molecules are actively transported to the surface by inertial mixing, and more rapidly collide with the capture antibodies. Fig. 4 shows data for PSA assays performed by two scientists where the microtiter plates were static or orbitally shaken during the incubation steps. At CL signals where we are able to determine a robust signal per enzyme label (see Section 3.4)—corresponding to PSA concentrations of 32 fM to 354 fM— the mean ratio of signal from the shaken to unshaken condition was 10.2, ranging from 8.0 to 12.6. Table 1 shows the signals and imprecision at the different concentrations measured in these experiments.

Shaking at the sample incubation step was the dominant factor for high signals in the assay. Fig. S4 shows data from control experiments

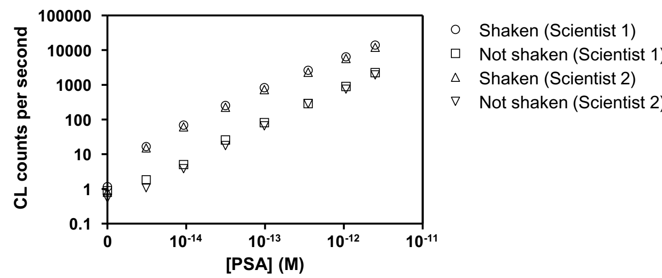

Fig. 4. Plot of CL counts per second against concentration of PSA when the plate was either shaken during incubation steps or was not shaken. Data from two different scientists for the two conditions are shown.

where shaking was not performed at the sample, detection antibody, and enzyme incubation steps. In all of the control experiments in which the sample step was not shaken, signals were significantly lower than the fully shaken assay. Even if the assay was not shaken at either or both of the labeling steps, high signals were observed, although the highest signals were observed when every step was shaken. These observations were expected as target analyte is present in limiting concentrations (< 1 pM), and requires active transport to the surface for maximum signals, whereas the labeling reagents are present in non-limiting concentrations (6.7 nM and 0.44 nM for detection antibody and SA-HRP, respectively), and do not require active transport (Section 3.5.3).

The higher capture efficiencies when shaken orbitally and sub-femtomolar sensitivity to enzyme label resulted in a highly sensitive assay for PSA. The LODs of the two shaken PSA assays shown in Fig. 4 were 90 aM and 67 aM (2.7 and 2.0 fg/mL). This sensitivity compares favorably to the most sensitive commercial PSA assay reported to date (50 aM or 1.5 fg/mL).(Rissin et al., 2010) The assay sensitivity is also comparable to the LOD of the enzyme assay, indicating that sensitivity is limited by the ability to detect the enzyme labels. For comparison purposes, the mean LOD of the PSA assay when the plate was not shaken was 840 aM or 25 fg/mL.

3.5.2. Theoretical models

We developed theoretical models for the kinetics of binding in the CL ELISA array in which the plates were either shaken orbitally or not shaken. In the following, we describe our model of antigen transport in the presence of complex flow generated by orbital shaking, and how we simulated three dimensional diffusion of antigen in an unshaken well.

3.5.2.1. COMSOL model of binding in an orbitally shaken plate. In the case of a plate being shaken orbitally during incubation, we developed two models to test, one based on a two-layer model assuming well-mixed liquids, and the other one based on a three-layer model assuming liquids that are well-mixed in bulk phase, but not well-mixed near the surface of the binding region due to viscous force.

The two-layer model divides the system into an antibody layer, where binding events occur, and homogeneous bulk phase (Fig. 5). We assumed that the bulk phase was well-mixed initially, such that the bulk antigen concentration was spatially constant throughout this layer, with the bulk antigen concentration decreasing over time due to antigen-antibody binding. We considered surface-averaged binding kinetics at each z value in the antibody layer in order to calculate the total number of captured antigens. Thus, one dimensional reaction-diffusion equations were employed to describe antigen diffusion and binding reactions in the antibody layer where inertial mixing by orbital shaking was no longer applied. Fig. 5 shows the one dimensional reaction-diffusion equations, and the initial and boundary conditions used for the antibody layer in a 600-μm array spot. We assumed that the capture antibody molecules were homogeneously distributed and fixed in the antibody layer; diffusion terms for the capture antibody and the

Table 1
CL signals and efficiency of detection of enzyme labels for CL ELISA for PSA run by two scientists with plates orbitally shaken or not shaken at incubation steps. Data were taken from the calibration curves plotted in Fig. 4. The number of labels detected was calculated from the CL signal per second less background normalized to the CL signal per second per molecule for signals in the quantifiable range (Fig. S3). The efficiency of detection was the ratio of detected enzyme labels to the total number of PSA molecules in the sample. n.d. = not determined.

			Scientist 1									Scientist 2								
			Shaken				Not shaken					Shaken				Not shaken				
[PSA] (pg/mL)	[PSA] (fM)	No. of molecules	CL signal/s	CV	No. of labels detected	Effic-iency.	CL signal/s	CV	No. of labels detected	Effic-iency.	shake/unshak-en ratio	CL signal/s	CV	No. of labels detected	Effic-iency.	CL signal/s	CV	No. of labels detected	Effic-iency.	shake/unshak-en ratio
75.1	2503	75,350,333	13,968.9	2%	n.d.	n.d.	2253.4	6%	n.d.	n.d.	n.d.	12,025.3	4%	n.d.	n.d.	1940.3	4%	n.d.	n.d.	n.d.
32.1	1070	32,200,997	6504.0	4%	n.d.	n.d.	893.6	4%	n.d.	n.d.	n.d.	5798.4	11%	n.d.	n.d.	757.3	2%	n.d.	n.d.	n.d.
10.6	354	10,642,702	2652.7	2%	4,106,471	38.6%	285.1	3%	462,896	4.3%	8.9	2303.0	7%	3,578,986	33.6%	287.9	7%	467,805	4.4%	7.7
2.9509	98.4	2,960,720	834.5	2%	1,322,856	44.7%	81.5	3%	141,252	4.8%	9.4	730.2	3%	1,160,686	39.2%	65.4	8%	116,377	3.9%	10.0
0.9480	31.6	951,153	256.3	3%	417,013	43.8%	26.0	8%	52,563	5.5%	7.9	226.3	1%	370,348	38.9%	18.0	8%	40,051	4.2%	9.2
0.2780	9.3	278,931	69.0	4%	120,939	43.4%	5.1	13%	n.d.	n.d.	n.d.	62.2	7%	110,722	39.7%	3.8	5%	n.d.	n.d.	n.d.
0.0930	3.1	93,310	16.7	12%	36,526	39.1%	1.8	4%	n.d.	n.d.	n.d.	15.2	10%	34,658	37.1%	1.1	7%	n.d.	n.d.	n.d.
0	0	0	1.2	10%	–	–	0.9	16%	–	–	–	0.8	36%	–	–	0.5	3%	–	–	–

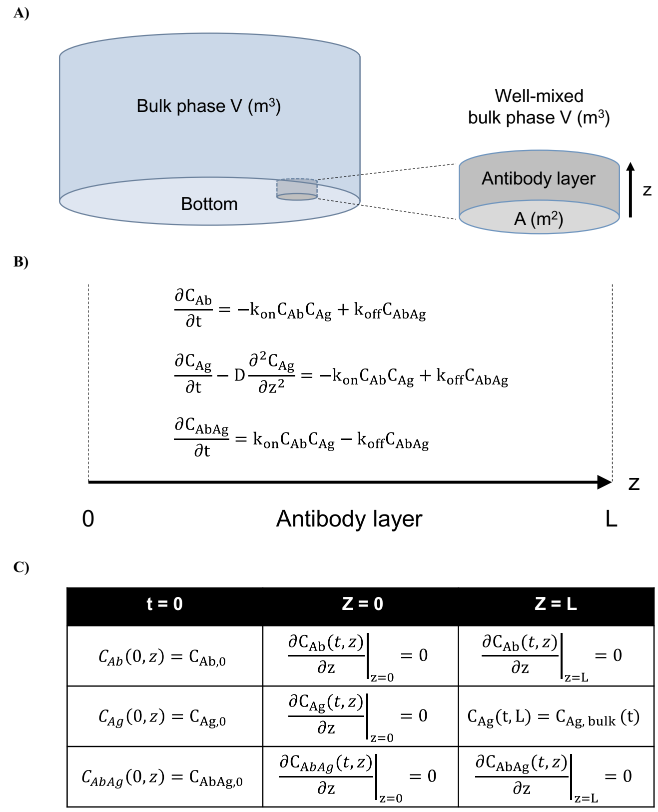

Fig. 5. Two-layer, well-mixed model for the antigen capture step in a shaken ELISA. A) Geometry of the well; B) Reaction-diffusion equations; C) Initial and boundary conditions. For the model of the ELISA for PSA, the initial conditions used were: $C_{Ab,\,0} = 14.03$ mol m^{-3}, $C_{Ag,\,0} = 3.53 \times 10^{-10}$ mol m^{-3} or 3.15×10^{-11} mol m^{-3}, and $C_{AbAg,\,0} = 0$ mol m^{-3}.

antibody-antigen complexes were, therefore, not required. Antigen molecules can diffuse from the bulk phase into the antibody layer and bind to antibody molecules, so there is a diffusive mass transport term ($D\frac{\partial^2 C_{Ag}}{\partial z^2}$) in the antigen reaction-diffusion equation. In the initial state, there are fixed amounts of antibody and antigen in the antibody layer, and there is no antigen-antibody complex. Both layers have the same initial concentration of antigen. The concentration of the antigen decreases as the antigens bind to the antibodies, and diffusion of antigen from the bulk phase to the antibody layer occurs. At the bottom of the well, there is neither generation nor consumption of antigen (zero molar flux). At the interface of the antibody layer and the bulk phase, the concentration of antigen ($C_{Ag}|_{z=L}$) is equal to bulk antigen concentration ($C_{Ag,\,bulk}$); this value can be obtained by subtracting captured antigen concentration from initial bulk antigen concentration. The corresponding two-layer models for the CL ELISA steps of biotinylated detection antibody binding to captured antigen and binding of SA-HRP to the captured detection antibody are shown in Fig. S5 and Fig. S6, respectively.

The three-layer model assumes an additional concentration boundary layer between the antibody layer and the bulk phase as shown in Fig. 6. This concentration boundary layer can act as a diffusional barrier that can reduce the mass transport rate of antigen from the bulk phase, slowing the rate of capture compared to the two-layer model. We assumed that this layer would be thin enough to have a linear concentration profile. The reaction-diffusion equations, and initial and boundary conditions in the three-layer model are the same as in the two-layer model, except for the inward flux condition at z = L, replacing the equal concentration condition ($C_{Ag}|_{z=L} = C_{Ag,\,bulk}$). Using the linearity of the concentration profile, the antigen molar flux ($N_{Ag,\,z}$) from the bulk phase is calculated by

A)

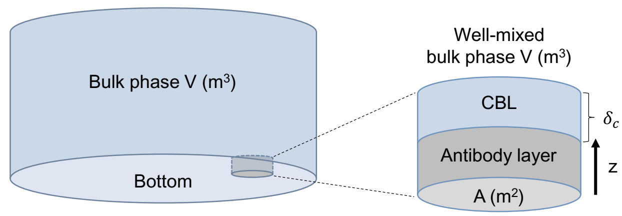

B)

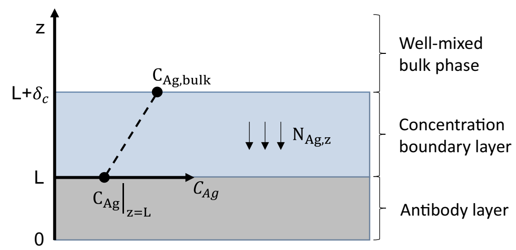

$$N_{Ag,z} = -D\frac{\partial C_{Ag}}{\partial z}\bigg|_{z=L} = \frac{D}{\delta_c}\left(C_{Ag,bulk} - C_{Ag}\big|_{z=L}\right)$$

Fig. 6. Three-layer, not well-mixed model for the antigen capture step in a shaken ELISA. A) Geometry of the well, including concentration boundary layer (CBL); B) Initial and boundary conditions specific to this model. Other reaction-diffusion equations, and initial and boundary conditions are the same as Fig. 5.

$-D\frac{\partial C_{Ag}}{\partial z}\Big|_{z=L} = \frac{D}{\delta_c}(C_{Ag,bulk} - C_{Ag}|_{z=L})$, where δ_c is the thickness of concentration boundary layer. The corresponding three-layer models for the assay steps of biotinylated detection antibody binding to captured antigen and binding of SA-HRP to the captured detection antibody are shown in Fig. S5 and Fig. S6, respectively.

To estimate a theoretical value of δ_c, we first calculated an order-of-magnitude estimate of the momentum boundary layer thickness (δ_m), as described by Alpresa et al. (2018a, 2018b) by using $\delta_m \approx \sqrt{\frac{\nu}{\omega}} = 135\ \mu m$, where ν is the kinematic viscosity ($= 1 \times 10^{-6}\ m^2/s$ for water at 20 °C) and ω is the angular velocity ($= 525$ rpm ≈ 55 rad/s). The concentration boundary layer thickness, δ_c, can then be estimated using the Schmidt number, Sc, that is a ratio of momentum diffusivity and mass diffusivity: $Sc = \frac{\nu}{D} \approx 11{,}800$. For liquid systems, Sc is commonly $\gg 1$, which signifies that the momentum boundary layer is greater than the concentration boundary layer. The relationship between Sc, δ_m, and δ_c can be modeled as $\frac{\delta_m}{\delta_c} \approx Sc^n$, where n can be set to $n = \frac{1}{3}$ for $Sc \gg 1$, because the flow regime in the orbitally shaken well is laminar flow ($Re = R^2\omega/\nu = 545$).(Merk, 1959) The thickness of the concentration boundary layer, therefore, was estimated as $\delta_c \approx 6\ \mu m$. We compared this estimate with an effective δ_c obtained by comparing simulation results for time course SA-HRP binding to a spotted biotinylated antibody with experimental data (Section 3.5.3).

3.5.2.2. COMSOL model of binding in an unshaken plate. For a plate that is not shaken during incubation, antigen molecules are transported from upper bulk phase to the capture surface solely by diffusion. Given that the rate of diffusion is relatively slow compared to binding kinetics and that the binding region is not at the center of the well, a non-symmetrical concentration gradient is generated in the bulk phase; we, therefore, considered 3D diffusion throughout the entire volume of the well. Fig. 7 shows the 3D diffusion equation for antigen, and initial and boundary conditions for the unshaken well. To model the consumption and generation of antigen in the antibody layer, we used molar flux of antigen on the antibody spot as shown in Fig. 7. For any other surfaces, we applied no flux conditions. The corresponding unshaken models for the assay steps of biotinylated detection antibody binding to captured antigen and binding of SA-HRP to the captured detection antibody are shown in Fig. S7.

A)

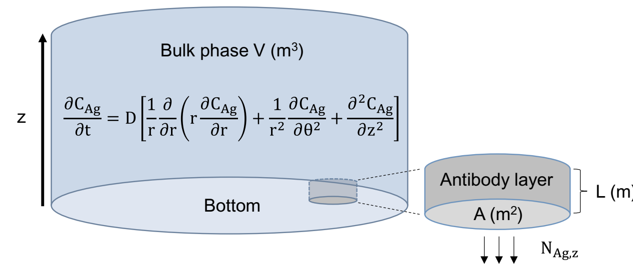

B)

t = 0	On antibody spot	Other boundaries
$C_{Ag}(0,r,\theta,z) = C_{Ag,0}$	$N_{Ag,z} = -D\frac{\partial C_{Ag}}{\partial z} = L\frac{\partial C_{Ag,l}}{\partial t} = -Lk_{on}C_{Ab,0}C_{Ag,l} + Lk_{off}C_{AbAg,l}$	$N_{Ag,r} = 0$ $N_{Ag,\theta} = 0$ $N_{Ag,z} = 0$

Fig. 7. 3D diffusional model for the antigen capture step in an ELISA that is not shaken. A) Geometry of the well and kinetic binding equations; B) Initial and boundary conditions. $C_{Ag,\,l}$ is the concentration of antigen in antibody layer. We multiplied the reaction rate by L to convert volumetric reaction rate ($mol\ m^{-3}\ s^{-1}$) in the antibody layer to molar flux ($mol\ m^{-2}\ s^{-1}$) at the antibody spot.

3.5.3. Comparison of experimental data and theoretical models

We first compared the theoretical models for a shaken plate from Section 3.5.2 to the kinetic data of SA-HRP binding to a spotted biotinylated antibody (Fig. S1). Details of the two- and three-layer models for this assay, where SA-HRP is used as antigen and a biotinylated antibody is used as a capture antibody, are shown in Fig. S8. Fig. 8 shows theoretical curves for the binding of 35 fM of SA-HRP as a function of time for two- and three-layer models of a shaken plate, assuming 3 biotins per detection antibody, a range of values of δ_c, and the physico-chemical parameters listed in Table S1. These data indicate that the capture kinetics in an orbitally shaken well are not predicted assuming a well-mixed solution, and that a three-layer model is more appropriate to understand the kinetics of binding. The experimental binding data were best fitted assuming $\delta_c = 8\ \mu m$, slightly greater than the value ($\delta_c = 6\ \mu m$) predicted from the estimate of momentum boundary layer thickness in orbitally shaken wells (Section 3.5.2.1).

Fig. 9 shows theoretical binding curves for the three steps of the PSA assay, i.e., capture of PSA by capture antibodies, labeling of PSA by biotinylated detection antibodies, and labeling of biotinylated detection antibodies by SA-HRP. For each step, theoretical curves are shown for

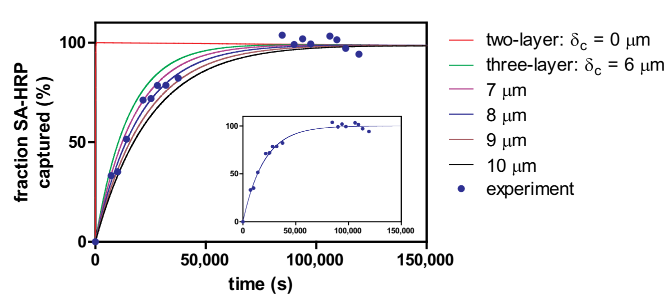

Fig. 8. Plot of fraction of molecules of SA-HRP captured against incubation time for a solution containing 35 fM SA-HRP incubated with a spotted biotinylated antibody. The experimental data are shown in blue circles based on the data from **Fig. S1**. The solid lines are fit to these data based on either the well-mixed, two-layer model, or the three-layer model using 5 different thickness of the concentration boundary layer (δ_c). The experimental data were best fitted by the three-layer model with $\delta_c = 8\ \mu m$ (inset plot). The capture efficiency extrapolated from this fit for a 5 h incubation was 59.4%. (For interpretation of the references to colour in this figure legend, the reader is referred to the web version of this article.)

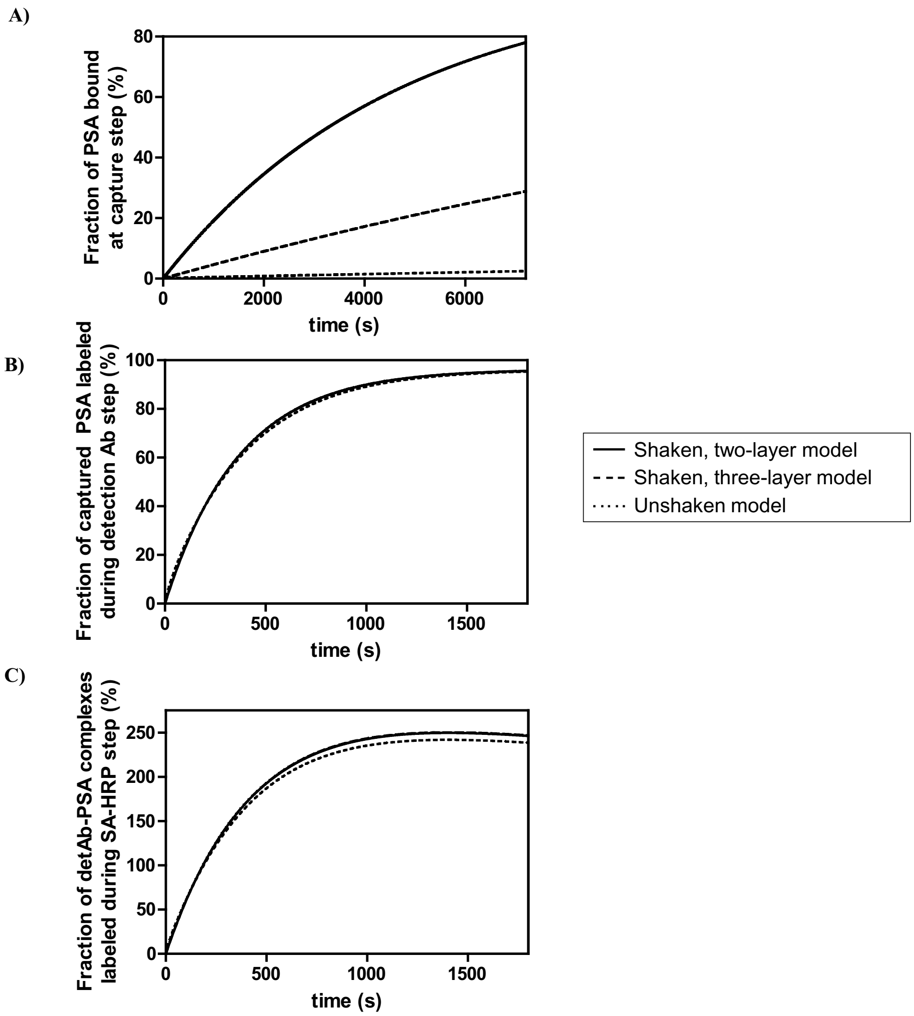

Fig. 9. Predicted efficiencies from three theoretical models of the three steps of the CL ELISA array for PSA. Plots of predicted efficiencies of the shaken, two-layer (solid line), shaken, three-layer (long dash) and, unshaken (short dash) models for: A) capture of PSA molecules in the sample incubation step; B) labeling of the captured PSA molecules during incubation with detection antibodies, and C) labeling of the captured detection antibodies during incubation with SA-HRP. $\delta_c = 8\,\mu m$ for the shaken, three-layer model. Predictions are based on [PSA] = 31.5 fM.

the shaken plate (two-layer and three-layer models) and the unshaken plate, based on the physico-chemical parameters listed in Table S1; the three-layer model assumed $\delta_c = 8\,\mu m$, corresponding to the fit of SA-HRP binding (Fig. 8) and close to the value predicted by theory. For the first step, the concentration of binding reagent at the surface was equal to the concentration of the printed capture antibodies. The subsequent two steps used concentrations of binding reagents (PSA and biotinylated detection antibodies, respectively) determined from the theoretical model of the prior step. We also took into account the washing steps where detection antibodies were free to dissociate from the bound immunocomplexes.(Chang et al., 2012) Table S2 shows the efficiencies of each step for the specific incubation times of the PSA assays performed here.

Two parameters in this model merit specific comment, i.e., the number of biotins on the detection antibody and the off rate of the detection antibody. We modeled the data using 3 biotin groups per detection antibody based on experimental quantification of the average number of biotins conjugated to the antibodies. In theory, therefore, each captured PSA molecule could be labeled by up to 3 molecules of SA-HRP. As a result, for example, the efficiency of the SA-HRP step for the two-layer model was > 100% (Fig. 9C). This situation is in contrast to our modeling of the Simoa bead assay,(Chang et al., 2012) where the very high sensitivity to enzyme labeled allowed us to kinetically constrain the enzyme label step to minimize backgrounds, such that the average number of enzyme labels per PSA molecule was < 1. For the CL ELISA, the lower sensitivity to enzyme requires higher labeling efficiencies to improve detection of the captured molecules, such that multiple molecules of SA-HRP label each detection antibody. For illustration, the Simoa assay for PSA incubates with SβG at 50 pM for 5 min, resulting in a predicted labeling efficiency of 7.4%,(Chang et al., 2012) whereas the CL ELISA incubates with SA-HRP at 440 pM for 30 min, resulting in a predicted labeling efficiency of 246% for the three-layer model (Table S2). We believe that the smaller size of SA-HRP (MW ≈ 113 kDa) compared to SβG (MW ≈ 700 kDa) makes binding of multiple enzyme conjugates to each detection antibody sterically more likely, as well as being predicted kinetically.

The theoretical models are particularly sensitive to the off rate of the detection antibodies. As we have described elsewhere,(Chang et al., 2012) the dissociation of the captured protein and streptavidin labeled enzymes occur very slowly in ELISA, but detection antibodies freely dissociate from the target protein at the surface, at relatively high rates. In our previous studies using the same detection antibody for PSA, we showed that the off rate of the detection antibody in the ELISA format was slower ($k_{off} \approx 1 \times 10^{-4}\,s^{-1}$) than the value determined using a biosensor technology ($k_{off} = 8.57 \times 10^{-4}\,s^{-1}$).(Chang et al., 2012) For greater accuracy, therefore, in the models presented here, we used the

Table 2
Comparison of efficiencies of theoretical models and experimental data of PSA CL ELISA. Efficiency = number of SA-HRP molecules bound/total number of PSA molecules in the sample.

	[PSA] = 31.5 fM	[PSA] = 353 fM
Shaken, two-layer model (A)	165.8%	165.7%
Shaken, three-layer model (δ_c = 8 μm) (B)	61.2%	61.0%
Shaken, experiment (C)	41.4%	36.1%
Not shaken, model (D)	4.8%	4.8%
Not shaken, experiment (E)	4.9%	4.4%
Ratio shaken, two-layer to not shaken models (= A/D)	34.5	34.5
Ratio shaken, three-layer to not shaken models (= B/D)	12.8	12.7
Ratio experiment, shaken to not shaken (= C/E)	8.5	8.2

off rate determined from the previous study using ELISA (Table S1).

We used the CL signal per second from these PSA assays and CL signal per second per molecule of SA-HRP to determine the efficiency of the CL ELISA array. Based on the extrapolated CL signal per second per molecule (Fig. S3), we determined the number of enzyme molecules detected for each PSA sample tested for the shaken and not shaken assays (Fig. 4 and Table 1) in the range of signals where signals per molecule could be reliably quantified (10–5000 CL counts per second). Table 1 shows the efficiency of detecting PSA molecules based on the ratio of number of molecules of SA-HRP detected and the number of molecules of PSA in each sample. From these data, the overall efficiencies of the shaken PSA assay for 2 h sample incubation times ranged from 34 to 45% (3.1–354 fM). For an unshaken PSA assay, the efficiencies ranged from 3.9–5.5% (31.6–354 fM). The mean ratio of detection efficiency of shaken to not shaken was 8.8 (range = 7.7–10.0).

Table 2 summarizes the overall efficiencies of the PSA assay predicted by the three models and the corresponding experimental efficiencies, based on the data in Table S2 and Table 1, respectively. For the shaken plate, the overall efficiencies predicted by three-layer model with δ_c = 8 μm are within a factor of 2 of the efficiencies determined experimentally, and much closer than the two-layer, well-mixed model. The fact that both the shaken PSA and SA-HRP assays were best modeled by the three-layer approach, suggests a model in which the solutions are not well-mixed and there is a concentration boundary layer is the most appropriate for CL ELISA. For the unshaken plate, the diffusion model (Section 3.5.2.2) predicted an overall efficiency very close to that of the experimental values. The ratio of efficiency between the three-layer shaken model and unshaken model (~12.7) was comparable to the ratio of shaken to unshaken plates determined experimentally (~8.5). We also note that the predictions of high efficiencies of the detection antibody and enzyme labeling steps by the model of the static plate verify the experimental observation that shaking is only essential at sample incubation (Fig. S4).

We believe that the discrepancies between theoretical and experimental data for the shaken plates indicate the challenges in modeling binding kinetics in complex fluidic systems. The discrepancies are also likely driven by uncertainty in the parameters used (e.g., k_{on} and k_{off} values), and by the effective binding capacity of the 3 biotin groups on the detection antibodies. For example, steric reasons could effectively reduce the concentration of biotin available to bind at the surface, bringing theory and experiment closer into line.

3.6. Sensitivity of a single-plex assay for IL-10, and detection in serum and plasma

We developed a single-plex (one spot arrayed) CL ELISA for IL-10 to demonstrate the sensitivity to a cytokine in plasma and serum. Fig. 10 shows a plot of CL signal as a function of [IL-10]. The average LOD for the IL-10 assay across five runs was 69 aM or 1.5 fg/mL of IL-10. This LOD is comparable to an assay for IL-10 based on Simoa (4 fg/mL or 190 aM).(Casaletto et al., 2018) The dynamic range of the assay was 4.6 logs.

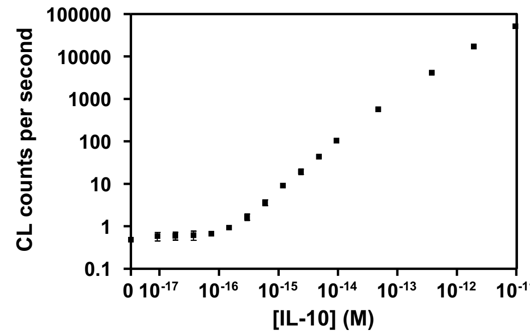

Fig. 10. Plot of CL counts per second against concentration of IL-10 for a single-plex CL array assay for IL-10.

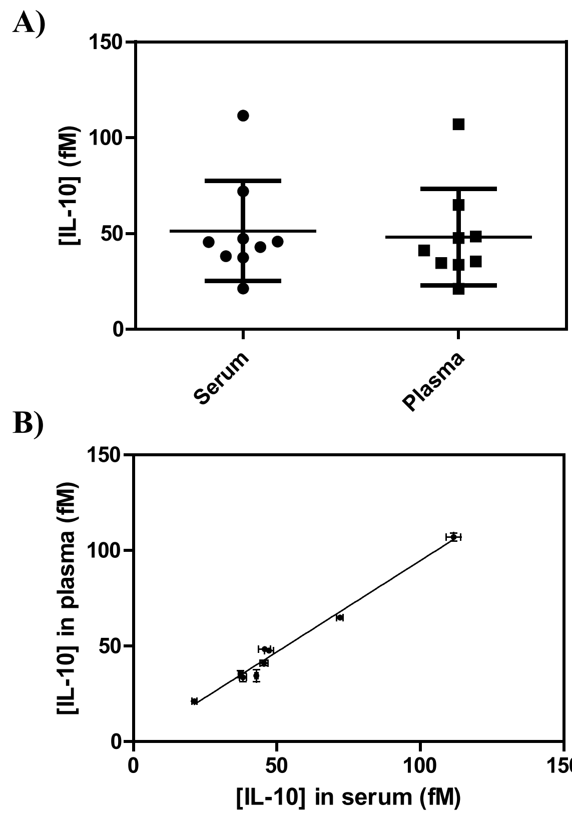

Fig. 11. A) Scatter plots of concentration of IL-10 determined using a single-plex CL array assay in the serum and plasma of 9 healthy donors. B) Correlation of the concentration of IL-10 determined using a single-plex CL array assay in the serum and plasma of 9 healthy donors.

We used this assay to measure IL-10 in matched serum and plasma samples from human donors. Fig. 11 shows a scatter plot of the concentration of IL-10 in these samples, and Table S3 shows the replicate data and precision of each measurement. The average concentration of IL-10 was 51.3 ± 26.2 fM (1.08 ± 0.549 pg/mL) and 48.2 ± 25.2 fM (1.01 ± 0.529 pg/mL) in serum and plasma, respectively. One matched serum and plasma sample was excluded from our analysis due to nonspecific signal arising from heterophilic interference of anti-bovine immunoglobulin (IgG) antibodies in the sample. Fig. S9 shows that spiking bovine IgG into this sample reduced signal by 74% in serum and 83% in plasma, whereas bovine IgG had no significant effect on other samples. Fig. 11 also shows that the correlation between the

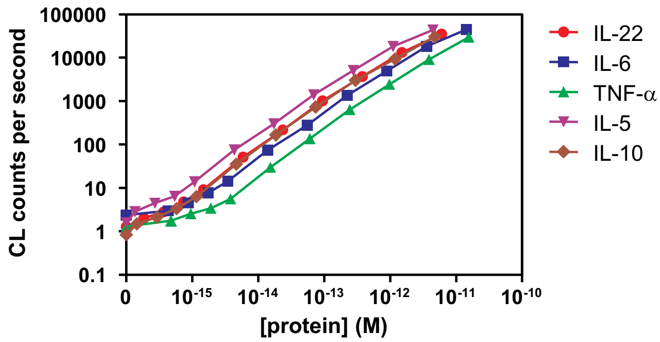

Fig. 12. Plots of CL counts per second against concentration of IL-22, IL-6, TNF-α, IL-5, and IL-10 for a 5-plex CL array assay.

concentration of IL-10 in serum and plasma was good ($r^2 = 0.98$; slope = 0.95). All serum and plasma sample measurements had CV < 10% (Table S3).

3.7. Sensitivity of a 5-plex assay for IL-5, IL-6, IL-10, IL-22, and TNF-α, and detection in serum and plasma

To demonstrate the sensitivity of detection of multiple cytokines simultaneously in plasma and serum, we developed a 5-plex CL ELISA array for IL-5, IL-6, IL-10, IL-22, and TNF-α. Fig. 12 shows plots of CL signals as a function of the 5 cytokines. The LODs of the assays were 56 aM (2.5 fg/mL), 237 aM (5.0 fg/mL), 69 aM (1.4 fg/mL), 88 aM (1.5 fg/mL), and 373 aM (9.5 fg/mL) for IL-5, IL-6, IL-10, IL-22, and TNF-α, respectively. The multiplex assay was used to measure these 5 cytokines in the same matched serum and plasma samples as tested in the IL-10 single-plex assay. Heterophilic blockers were included in the sample diluent, so no samples were excluded for non-specific signal. All cytokine concentrations in all samples were above both LOD and LLOQ. Fig. S10 shows scatter plots of the five cytokine concentrations in the serum and plasma samples, and Table S4 shows the average concentration of each cytokine across three replicates, the precision of each measurement, and the average concentrations across the donors. 86% of sample measurements had CV < 10%, and 94% of sample measurements had CV < 15% (Table S4). Fig. 13 shows that the correlations between concentration in serum and plasma was good for IL-5, IL-6, IL-10, and IL-22 (r^2 = 1.0, 0.97, 0.98, and 0.99 and slope = 1.1, 0.81, 0.99, and 0.77, respectively), but poor in TNF-α (r^2 = 0.56 and slope = 0.58).

Fig. 14 shows a comparison of the IL-10 concentrations of the matched serum and plasma samples between the single-plex and multiplex assay measurements. The sample exhibiting nonspecific signal in the single-plex assay was excluded from the correlation analysis. The correlation in concentration of IL-10 measured in single-plex versus multiplex format was good, with an r-squared value of 0.89 and a bias of +14.5% in single-plex measurements as compared to multiplex measurements.

4. Conclusions

We have characterized the sensitivity and binding kinetics of a multiplex ELISA based on chemiluminescence detection. The method allowed subfemtomolar detection of proteins in serum and plasma based on subfemtomolar sensitivity to the HRP enzyme label. The method had good precision and could be multiplexed readily based on the use of a high precision printing technology. We demonstrated the sensitivity and precision using two single plex assays and a 5-plex assay that enabled detection of proteins in the serum and plasma of healthy humans. Based on the current array configuration, the method should readily allow the development of assays for measuring up to 12 proteins simultaneously.

We also developed a quantitative model for the transport and binding of molecules at the arrays. The model took into account the active shaking of the microtiter plate, diffusion, and binding kinetics at the surface to predict the concentration of protein molecules captured and labeled at a spot in the array. The model compared favorably to experimental data for an assay for PSA where CL signals were converted to numbers of molecules. The ability to develop CL ELISA with very high sensitivities was, therefore, confirmed theoretically as well as experimentally.

For a technology that was first reported in 2001 demonstrating LODs for cytokines in the pg/mL range using well established reagents and signal generation system,(Moody et al., 2001) a natural question is where did the fg/mL sensitivity reported here—which compares favorably to the most sensitive immunoassays reported to date(Rissin et al., 2010)—derive from? In summary, the high sensitivity of the assay is a result of using a label detection method (enzyme-amplified chemiluminescence) that intrinsically has very high detection signal-to-noise for enzyme labels that produce many detectable molecules, married with a combination of improvements in several areas of the assay and instrumentation. Several of the advancements in the last 18 years have been characterized or demonstrated here, some have been reported elsewhere, and some are more speculative; all can be categorized as either maximizing SNR from enzyme labels, or maximizing the kinetics and specificity of binding.

SNR from enzyme labels in the CL array assay has been maximized via 5 factors:

1) CL is intrinsically a very high signal-to-noise detection method, as photons are only generated from the labels themselves (assuming a completely light-tight housing for the imager), unlike fluorescence, for instance, where excitation light can lead to detectable photons that contribute to background and noise. Enzymes further increase SNR by producing thousands of CL molecules for each protein labeled with an enzyme;
2) In principle, the sensitivity to enzyme is only limited by the efficiency of the collection options, and the quantum efficiency and noise of the camera used to image the arrays. Scientific CCD cameras have undergone dramatic improvements in recent years, and further improvements to the sensitivity of the CL method are expected as cameras improve;
3) The plates are imaged through an optically flat interface (the transparent bottom of the well in the microtiter plate) that helps reduce background compared to imaging through the meniscus by minimizing the scatter of the emitted light;
4) Long exposure times, as characterized here, can help to maximize the collection of CL and improve signal-to-noise;
5) Image analysis algorithms described here that are based on greater computational capacity can be used to maximize SNR.

The efficiency and reproducibility of kinetics of binding of enzyme labels has been optimized in the CL ELISA array via a further 4 factors:

1) The use of small area binding features via microarray printing described here concentrates the signal generated on a small area of the sensor, maximizing SNR as described by Ekins (2013)
2) The activity (binding capacity) of antibodies within the spot on the surface is impacted by the method of printing. The process used to array spots of antibodies here is based on droplet formation on the end of ultra-smooth steel pins and gentle contact of the pin with the substrate. We believe that this approach more effectively retains the activity of the printed antibodies compared to more invasive printing methods, such as inkjet printing;(Austin and Holway, 2011)
3) As described in section 3.1 and elsewhere, (United States Patent Application 13/677113, 2013) the use of a circular array of antibodies reduces the spot-to-spot variability associated with rectangular grids of antibody spots that are commonly used in plate-based

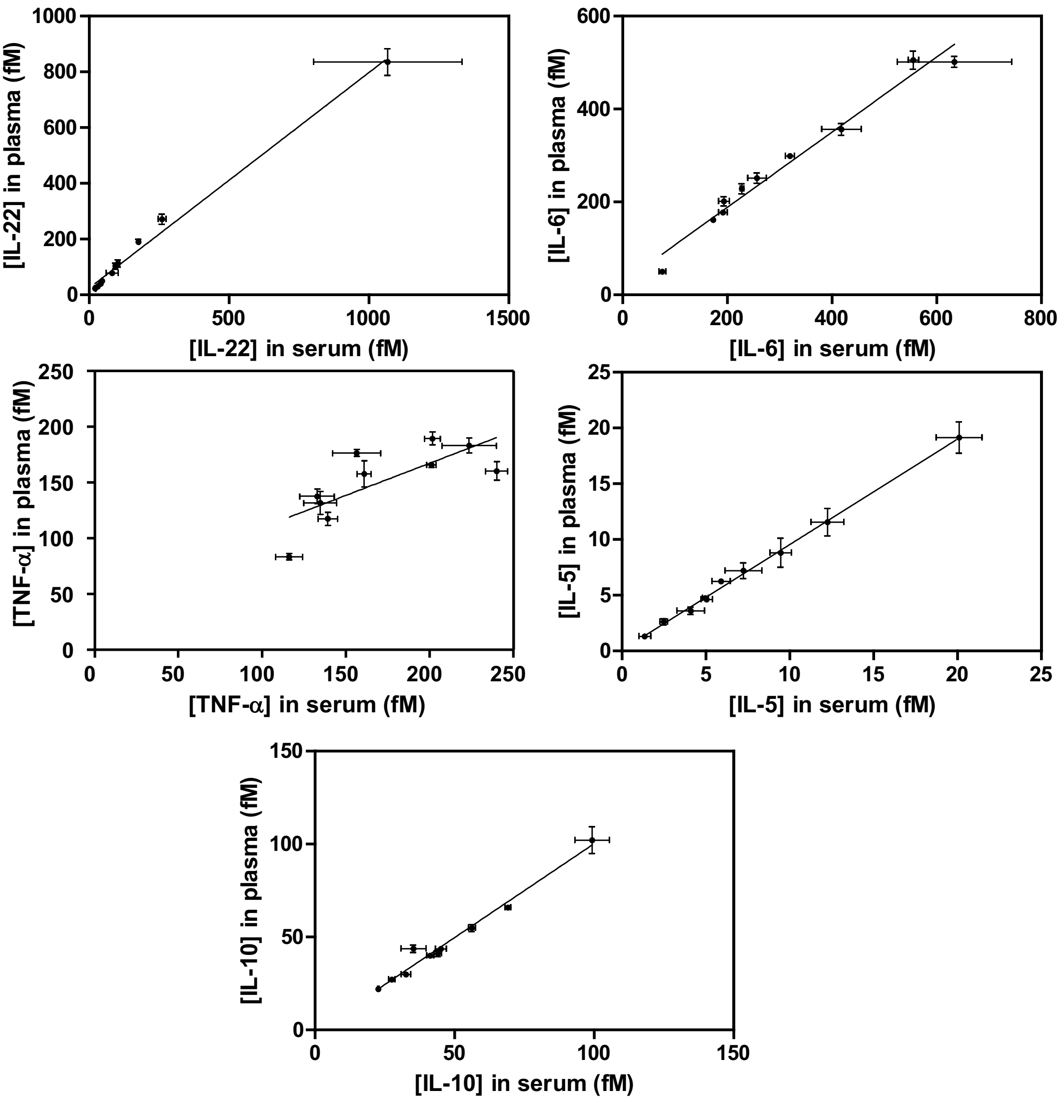

Fig. 13. Correlation plots of the concentration of 5 cytokines in the serum and plasma of 10 healthy donors determined using a 5-plex CL ELISA array.

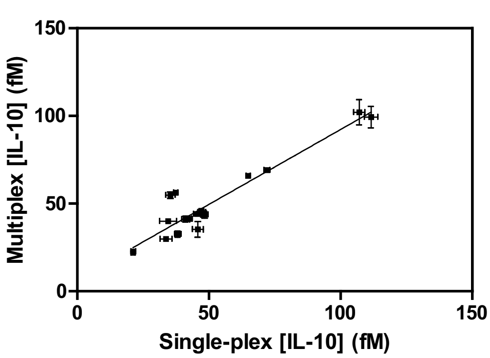

Fig. 14. Correlation of the concentration in the serum and plasma of 9 healthy donors of IL-10 determined using single-plex and 5-plex CL ELISA arrays.

immunoassay arrays;

4) As described above, shaking of the microtiter plate reduces the limitations of diffusion-limited binding of molecules at the surface of the array. Orbital shaking results in a ~10-fold increase capture of molecules, making the detection system the primary limiting factor of sensitivity, not binding kinetics.

The specificity of the signal from the enzyme labels has been optimized in the CL ELISA array via 2 factors:

1) To achieve low assay backgrounds (and consequently low noise) it is important to effectively and evenly block the antibody binding surface with proteins that resist non-specific binding of non-target molecule components of the sample;
2) High efficiency washing and removal of residual volume of enzyme label—as demonstrated here with highly dilutative wash procedures—is important to ensure that the enzyme signal is specific to labeled target antigen molecules.

Based on our characterization of the sensitivity and binding kinetics of the CL ELISA array, we believe that this assay system is suitable for applications in diagnostics and testing of samples from pre-clinical and clinical development of therapeutics that require high sensitivity to multiple proteins. The approach also holds promise for enabling further improvements to the sensitivity of multiplex immunoassays.

Acknowledgements

We are grateful to the Quanterix manufacturing group for preparing the plates spotted with biotinylated detection antibody. We thank

Professor William M. Deen (MIT) for providing feedback on the ELISA binding kinetics model, and David Fournier for helpful discussions on the kinetics of the enzyme-substrate reaction. We thank Anne Tsimboukis (atsimboukis@aol.com) for rendering Fig. 1.

Declaration of Competing Interest

C.I.T., D.M.R., J.M.J., S.D., S.Y., S.N., and D.C.D. are employees of Quanterix Corporation, and own stock or stock options in Quanterix Corporation. B.R. is a consultant to Quanterix. Quanterix manufactures and sells instrumentation and assay kits based on the technology described in this manuscript. S.K., K.-J.S., and H.D.S. have no competing interests to declare.

Appendix A. Supplementary data

Supplementary data to this article can be found online at https://doi.org/10.1016/j.jim.2019.112643.

References

Alpresa, P., Sherwin, S., Weinberg, P., van Reeuwijk, M., 2018a. Orbitally shaken shallow fluid layers. I. Regime classification. Phys. Fluids 30, 032107.
Alpresa, P., Sherwin, S., Weinberg, P., van Reeuwijk, M., 2018b. Orbitally shaken shallow fluid layers. II. An improved wall shear stress model. Phys. Fluids 30, 032108.
Austin, J., Holway, A.H., 2011. Contact printing of protein microarrays. Methods Mol. Biol. 785, 379.
Backen, A.C., Cummings, J., Mitchell, C., Jayson, G., Ward, T.H., Dive, C., 2009. Fit-for-purpose' validation of SearchLight multiplex ELISAs of angiogenesis for clinical trial use. J. Immunol. Methods 342, 106.
Casaletto, K.B., Elahi, F.M., Fitch, R., Walters, S., Fox, E., Staffaroni, A.M., Bettcher, B.M., Zetterberg, H., Karydas, A., Rojas, J.C., Boxer, A.L., Kramer, J.H., 2018. A comparison of biofluid cytokine markers across platform technologies: correspondence or divergence? Cytokine 111, 481.
Chandra, P.E., Sokolove, J., Hipp, B.G., Lindstrom, T.M., Elder, J.T., Reveille, J.D., Eberl, H., Klause, U., Robinson, W.H., 2011. Novel multiplex technology for diagnostic characterization of rheumatoid arthritis. Arthritis Res. Ther. 13, R102.
Chang, L., Rissin, D.M., Fournier, D.R., Piech, T., Patel, P.P., Wilson, D.H., Duffy, D.C., 2012. Single molecule enzyme-linked immunosorbent assays: theoretical considerations. J. Immunol. Methods 378, 102.
Chen, G., Jin, M., Du, P., Zhang, C., Cui, X., Zhang, Y., Wang, J., Jin, F., She, Y., Shao, H., Wang, S., Zheng, L., 2017. A review of enhancers for chemiluminescence enzyme immunoassay. Food Agric. Immunol. 28, 315.
Claudon, A., Vergnaud, P., Valverde, C., Mayr, A., Klause, U., Garnero, P., 2008. New automated multiplex assay for bone turnover markers in osteoporosis. Clin. Chem. 54, 1554.
Cohen, L., Walt, D.R., 2019. Highly sensitive and multiplexed protein measurements. Chem. Rev. 119, 293.
Cormier, M.J., Prichard, P.M., 1968. An investigation of the mechanism of the luminescent peroxidation of luminol by stopped flow techniques. J. Biol. Chem. 243, 4706.
Ekins, R., 2013. Ambient analyte assay. In: Wild, D. (Ed.), The Immunoassay Handbook, Fourth edition. Elsevier, Oxford, UK.
Ekins, R.P., Chu, F.W., 1991. Multianalyte microspot immunoassay–microanalytical "compact disk" of the future. Clin. Chem. 37, 1955.
Ekins, R., Chu, F., Micallef, J., 1989. High specific activity chemiluminescent and fluorescent markers: their potential application to high sensitivity and 'multi-analyte' immunoassays. J. Biolumin. Chemilumin. 4, 59.
Gorris, H.H., Walt, D.R., 2009. Mechanistic aspects of horseradish peroxidase elucidated through single-molecule studies. J. Am. Chem. Soc. 131, 6277.
Malekzadeh, A., Twaalfhoven, H., Wijnstok, N.J., Killestein, J., Blankenstein, M.A., Teunissen, C.E., 2017. Comparison of multiplex platforms for cytokine assessments and their potential use for biomarker profiling in multiple sclerosis. Cytokine 91, 145.
McDonald, M.L., Parsons, J.K., 2016. 4-Kallikrein Test and Kallikrein markers in prostate cancer screening. Urol. Clin. North Am. 43, 39.
Mendoza, L.G., McQuary, P., Mongan, A., Gangadharan, R., Brignac, S., Eggers, M., 1999. High-throughput microarray-based enzyme-linked immunosorbent assay (ELISA). Biotechniques 27, 778.
Merk, H.J., 1959. Mass transfer in the laminar boundary layer along a flat plate calculated by means of the integral method. Appl. Sci. Res. 261 A8.
Moody, M.D., Van Arsdell, S.W., Murphy, K.P., Orencole, S.F., Burns, C., 2001. Array-based ELISAs for high-throughput analysis of human cytokines. Biotechniques 31, 186.
O, D.F., El Aalamat, Y., Waelkens, E., De Moor, B., D'Hooghe, T., Fassbender, A., 2017. Multiplex immunoassays in endometriosis: an array of possibilities, front. Biosci. (Landmark Ed.) 22, 479.
Purushothama, S., Dysinger, M., Chen, Y., Österlund, K., Mora, J., Chunyk, A.G., Peloquin, R., 2018. Emerging technologies for biotherapeutic bioanalysis from a high-throughput and multiplexing perspective: insights from an AAPS emerging technology action program committee. Bioanalysis 10, 181.
Rissin, D.M., Kan, C.W., Campbell, T.G., Howes, S.C., Fournier, D.R., Song, L., Piech, T., Patel, P.P., Chang, L., Rivnak, A.J., Ferrell, E.P., Randall, J.D., Provuncher, G.K., Walt, D.R., Duffy, D.C., 2010. Single-molecule enzyme-linked immunosorbent assay detects serum proteins at subfemtomolar concentrations. Nat. Biotechnol. 28, 595.
Rivnak, A.J., Rissin, D.M., Kan, C.W., Song, L., Fishburn, M.W., Piech, T., Campbell, T.G., DuPont, D.R., Gardel, M., Sullivan, S., Pink, B.A., Cabrera, C.G., Fournier, D.R., Duffy, D.C., 2015. A fully-automated, six-plex single molecule immunoassay for measuring cytokines in blood. J. Immunol. Methods 424, 20.
Schlichting (Ed.), 2017. Boundary-Layer Theory, 9th Ed. pp. 29–36.
Schweitzer, B., Wiltshire, S., Lambert, J., O'Malley, S., Kukanskis, K., Zhu, Z., Kingsmore, S.F., Lizardi, P.M., Ward, D.C., 2000. Immunoassays with rolling circle DNA amplification: a versatile platform for ultrasensitive antigen detection. Proc. Natl. Acad. Sci. U. S. A. 97, 10113.
Spurrier, B., Honkanen, P., Holway, A., Kumamoto, K., Terashima, M., Takenoshita, S., Wakabayashi, G., Austin, J., Nishizuka, S., 2008. Protein and lysate array technologies in cancer research. Biotechnol. Adv. 26, 361.
Tarhini, A.A., Lin, Y., Yeku, O., LaFramboise, W.A., Ashraf, M., Sander, C., Lee, S., Kirkwood, J.M., 2014. A four-marker signature of TNF-RII, TGF-α, TIMP-1 and CRP is prognostic of worse survival in high-risk surgically resected melanoma. J. Transl. Med. 12, 19.
United States Patent Application, 2013. 13/677113.
US Patent, 2014. 8,811,704.
Veitch, N.C., 2004. Horseradish peroxidase: a modern view of a classic enzyme. Phytochemistry 65, 249.
Vitt, J.E., Johnson, D.C., Engstrom, R.C., 1991. The effect of electrode material on the electrogenerated chemiluminescence of luminol. J. Electrochem. Soc. 138, 1637.
Weeks, I., Kricka, L.J., Wild, D., 2013. Signal generation and detection systems (excluding homogeneous assays). In: Wild, D. (Ed.), The Immunoassay Handbook, Fourth edition. Elsevier, Oxford, UK.
Wiese, R., Belosludtsev, Y., Powdrill, T., Thompson, P., Hogan, M., 2001. Simultaneous multianalyte ELISA performed on a microarray platform. Clin. Chem. 47, 1451.
Wild, D. (Ed.), 2013. The Immunoassay Handbook, Fourth edition. Elsevier, Oxford, UK.
Wilson, J.J., Burgess, R., Mao, Y.Q., Luo, S., Tang, H., Jones, V.S., Weisheng, B., Huang, R.Y., Chen, X., Huang, R.P., 2015. Antibody arrays in biomarker discovery. Adv. Clin. Chem. 69, 255.